12-2018

Remote Characterization of Physical Surface Characteristics of Mars Using Diurnal Variations in Apparent Thermal Inertia

Cameron Blake McCarty
University of Tennessee, cmccar11@vols.utk.edu

To the Graduate Council:

I am submitting herewith a thesis written by Cameron Blake McCarty entitled "Remote Characterization of Physical Surface Characteristics of Mars Using Diurnal Variations in Apparent Thermal Inertia." I have examined the final electronic copy of this thesis for form and content and recommend that it be accepted in partial fulfillment of the requirements for the degree of Master of Science, with a major in Geology.

Jeff Moersch, Major Professor

We have read this thesis and recommend its acceptance:

Joshua P. Emery, Christopher M. Fedo

Accepted for the Council:
Carolyn R. Hodges

Vice Provost and Dean of the Graduate School

(Original signatures are on file with official student records.)

Remote Characterization of Physical Surface Characteristics of Mars Using Diurnal Variations in Apparent Thermal Inertia

A Thesis Presented for the

Master of Science

Degree

The University of Tennessee, Knoxville

Cameron Blake McCarty

December 2018

Dedication

Mom,
I'll love you forever,
I'll like you for always.

Hannah,
You are the rock of stability in this
ocean of stress that's been grad school.

Laika,
Woof.

Honor the past,
Acknowledge the present,
Salute the future.
-Ron Anderson

Acknowledgements

I first want to express my appreciation for Jeff Moersch, my research advisor. His rigorous attention to detail has been incredibly valuable over this journey. Chris Fedo and Josh Emery have been a constant source of knowledge and academic advice. Other instructors who have always been available and insightful include: Hap McSween, Devon Burr, Annette Engel, Linda Kah, Larry Taylor, Ed Perfect, Brad Thomson, Nick Dygert, Molly McCanta, and Anna Szynkiewicz. Furthermore, this also couldn't have been possible without the reviews, discussions, late night study sessions, and general emotional rock provided by Audrey Martin, Michael Phillips, Jessi Ende, Sam Gwizd, Chad Melton, Cameron Hughes, Ariana Boyd, and Emily Neild. Many other friends have helped throughout the years including my second family at the Coca-Cola Space Science Center, specifically Shawn Cruzen and Tina Cross for help above and beyond what was asked. My friends back home: Matt Bartow, Cole Downey, Daniel Kunze, John Hood, David Stillwell, Zach and Cheryl Coker, Matt and Emily Perry, and Quinn and Michelle O'Brien. A huge thank you to my family who have been supportive of me and my dreams of space since I was a small child. And of course, Hannah Klein, who has kept me laughing, focused, and sane ever since I dragged her to Knoxville, so I could pursue my dream. I'm so grateful for my fellows on the Mars Exploration Rover Team who showed me the joys of working on another planet. Finally, I would like to thank the THEMIS team, without whom my research would not have been possible.

Abstract

Analysis of the Martian surface today can provide insight into the processes that may have affected it over its history. Information about the physical surface characterization of a region can help determine the degree of sorting it has experienced and/or its geologic maturity. Sub-resolved "checkerboard" mixtures of materials with different horizontal thermal inertia mixtures can lead to differences in the apparent thermal inertia values inferred from night and day radiance observations. Standard methods for deriving thermal inertia from orbit via the THermal EMission Imaging System (THEMIS) can give values for the same location that vary by as much as 20% between images (Fergason et al., 2006b). Such methods assume that each pixel contains material of a single, uniform thermal inertia. Here, it is proposed that if a mixture of low and high apparent thermal inertias is present within a pixel, the inferred thermal inertia will be strongly dominated by the thermal inertia of whichever surface is warmer at the time of the measurement. This effect will result in a change in thermal inertia values inferred from measurements taken at different times of day and night. Therefore, a correlation is hypothesized between the magnitude of diurnal variations in apparent thermal inertia values and the degree of non-uniformity of thermal inertias present in a given pixel location.

Preliminary work has shown that the magnitude of such diurnal variation in inferred thermal inertias is sufficient to detect geologically useful differences in surfaces mixtures. Mapping the difference in apparent thermal inertias from day and night THEMIS observations may prove to be a new way of distinguishing surfaces that have relatively uniform thermal inertias from those that have mixed thermal inertias.

Table of Contents

List of Figures

1. Background

1.1. Sediments on Mars

For billions of years on Mars, the dominant geologic processes have been sedimentary processes and impact gardening. As a result, detailed knowledge of the sediments at any given location is critical in the selection of landing sites for Martian exploration or evaluating any landscape that may have undergone sorting processes. For example, workers evaluating potential landing sites need to know the surface distribution of boulders within a given rover landing site before it is selected to evaluate the scientific potential as well as traversability (e.g., Grant et al., 2004, 2011). Well-sorted materials are more mature than those that are poorly sorted (Folk, 1974), and the degree of sedimentary sorting therefore provides information about a surface's geologic history. It is generally not possible to determine detailed grain properties from orbital images, and *in-situ* measurements are only available for a few small areas on Mars. Sedimentary sorting is a key observation for assessing whether the surface modification process in question was/is lacustrine, fluvial, alluvial, aeolian, or another mechanism.

It should be noted that orbital data cannot explain an entire geologic history by themselves; they must be taken in context with other properties of the area. On Mars, explaining the geologic history becomes a much more difficult issue, as data collection on Mars is much more limited than that on Earth. Data and samples can easily be collected in the field here on Earth, however on Mars, rovers have only explored a small portion of the surface. While this limited data can be supplemented with orbital systems, both suffer from resolution and data volume constraints. From a global sedimentary perspective, much of what is known regarding Martian grain sizes comes from the Thermal Emission

Spectrometer (TES) (Christensen et al., 2001) and the THermal EMission Imaging System (THEMIS) (Christensen et al., 2004). Standard thermophysical analysis methods used with both datasets rely on the assumption that the calculated thermal inertia for each of their pixels (3x6-km and 100x100-m respectively) are uniform. The purpose of the present work is to test the hypothesis that sub-pixel mixing of surfaces with varying thermal inertias will yield diurnally-variable apparent thermal inertias on the full-pixel scale, and that this variation is of sufficient magnitude to be observable in THEMIS data.

Here, the term "apparent thermal inertia" is used to denote the thermal inertia value inferred from a single time-of-day measurement under the assumption of a horizontally homogeneous thermal inertia pixel. This concept is distinct from the physical property of thermal inertia (herein referred to as "absolute thermal inertia"), which refers to a bulk material characteristic of the surface. Throughout this work, the terms homogeneity and heterogeneity will be used to reference the thermal inertia components. "Homogeneity" is not an indication that within the sub-pixel every component contains the exact same thermal inertia, but instead that the mixture is homogenous or heterogeneous with respect to the limit of detectability of the employed method and instrument. Furthermore, the term "components" will be used to describe the physical surface characteristics (herein referred to simply as "surfaces") of the region. For example, a pixel completely filled with well-sorted aeolian fine-grained material would be considered, in this context, a homogeneous surface, whereas a pixel that contains a mix of well-sorted aeolian fines plus boulders (or bedrock) would be considered a heterogeneous surface.

To confirm the viability of this hypothesis, the areas to be investigated herein will be those where *in-situ* measurements of the physical properties of the surfaces have been

made. These data do have constraints; the cameras onboard every rover have resolution limits for characterizing grains below certain sizes (Eibl et al., 2015), but sands around the rover have been analyzed by the Microscopic Imager (MI) and the Miniature Thermal Emission Spectrometer (miniTES), and were determined to be typically a fine sand with embedded particles in a bimodal distribution from 0.6 to 6 mm (Fergason et al., 2006a), which corresponds well with the laboratory measurements conducted by Iversen et al. (1976) that determined the most easily moved grain size on Mars to be 100-150 μm.

1.2. Radiance and Thermal Inertia

The TES and THEMIS instruments observe in the thermal infrared portion of the electromagnetic spectrum, measuring the target's spectral radiance. Through the Stefan-Boltzmann Law, the radiant flux of emitted radiance at all wavelengths over a surface per unit area can be calculated:

$$\Phi = \pi R = \sigma \epsilon T^4. \qquad [\mathrm{W/m^2}] \qquad [1]$$

Here Φ is the radiant emittance, σ is the Stefan-Boltzmann constant, R is the radiance, and ϵ is the emissivity; for any given brightness temperature T, an estimated radiant emittance may be calculated or vice-versa. Because the radiant emittance scales as the fourth power of the brightness temperature, a small increase in temperature can have a large increase in the radiant emittance. For example, take the average Martian surface temperature of 218 K: to increase the radiant emittance by 50%, the temperature only needs to rise to 259 K. Calculating the temperature on the surface of Mars also relies on a variety of factors which dictate the radiance the detector receives, so thermophysical models, (Kieffer, 2013; Putzig et al., 2013) must account for deviation in such variables as:

atmospheric opacity, slope, pits, diurnal variability, multiple sub-surface layering, rotation rate, stellar brightness, and orbital obliquity.

Thermal inertia (Kieffer et al., 1977) is an expression of how readily the temperature of an object responds to the presence of a heat source (usually insolation). It is expressed in thermal inertia units (tiu, defined as $J \cdot m^{-2} \cdot K^{-1} \cdot s^{-1/2}$) (Putzig, 2006) and is defined as the square root of the product of the thermal conductivity (k), density (ρ), and the specific heat capacity (C):

$$I \equiv \sqrt{k\rho C}. \qquad \text{[tiu]} \qquad [2]$$

On bodies with little or no atmosphere and low water content in the regolith, apparent thermal inertia on non-indurated surfaces is correlated with particle size (Kieffer et al., 1977; Presley and Christensen, 1997; Fergason et al., 2006a). In general, silt and other unconsolidated fines have lower absolute thermal inertias, sand-sized particles and consolidated fines have intermediate values, and boulder-sized rocks (and the thermophysically similar bedrock) have high absolute thermal inertias. By knowing the thermal inertia, and using the value of $1 \times 10^6\ J \cdot m^{-3}$ K for ρC (Christensen et al., 2001; Fergason et al., 2006a), equation 2 can be used to solve for k. Then the particle diameter, d, in microns, can be calculated by using the relationship established by Presley & Christensen (1997):

$$k = CP^{0.6} d^{-0.11 \log\left(\frac{P}{K}\right)}, \qquad \text{[W/(m·K)]} \qquad [3]$$

where $C \sim 0.0015$ and $K \sim 81{,}000$ torr respectively (1 torr = 133.3 Pa), and P is the average atmospheric pressure of 5 torr (Kieffer, 2013).

1.3. Thermal Inertia Variability

The above described relationship between the physical surface properties and thermal inertia is straightforward in homogeneous (single absolute thermal inertia) surfaces, but mixtures of variable (heterogeneous) surfaces are a non-trivial matter. When collecting data from orbit, the pixel resolution must be considered. Current methods for determining the apparent thermal inertia of the surface of Mars rely on the assumption that the components within a given pixel consists of a single thermal inertia. This is done through a two-step process: the radiance from a THEMIS pixel is input into a thermal model along with the appropriate conditions (time of day, time of year, location, albedo, slope, and tau) to calculate a temperature; second many thermal inertias are used to calculate diurnal temperature curves which are then matched against the temperature from the first step to find the closest curve. The thermal inertia which best matches the empirical value is the thermal inertia for that pixel.

However, the Stefan-Boltzmann Law dictates that grains of varying temperature will contribute to the overall radiant emittance disproportionately. Because spectral radiance is proportional to the 4^{th} power of temperature, the warmest components within a pixel of mixed thermal inertias will have a disproportionally high influence on the total radiant emittance of that pixel.

Figure 1 demonstrates this effect schematically. In this figure, it is assumed that three theoretical scenarios contain surfaces with varying thermal inertias surfaces corresponding to: homogeneous sand, homogeneous bedrock, and a heterogeneous mixture of the sand and bedrock. The calculated apparent thermal inertia for homogeneous surfaces does not vary between day and night data, which is to be expected. However,

when the mixed surface is observed at multiple times of day, the component that is warmest at any given time has a disproportionate influence over the apparent thermal inertia. The magnitude of this effect can be quantified by subtracting the calculated apparent thermal inertia in the predawn hours (when high thermal inertias dominate) from the calculated apparent thermal inertia during midday (when lower thermal inertias dominate). A large disparity between apparent thermal inertias derived from predawn and midday data would, therefore, indicate a greater degree of heterogeneity in the thermal inertia mixture, while a small or nonexistent variation in apparent thermal inertias would indicate a more homogenous thermal inertia mixture on the surface.

Previously, this phenomenon was studied for TES data (Putzig, 2006; Putzig et al., 2014; Putzig and Mellon, 2007a, 2007b), but the resolution of TES data is 3-km by 6-km and horizontal heterogeneity is almost guaranteed at such large scales. Unsurprisingly, all data collected with TES were found to exhibit heterogeneity and therefore this method was not explored further. By comparison, THEMIS has a resolution of 100-m per pixel, which outperforms TES by a factor of 1500 in area and may be more likely to resolve homogeneous surfaces.

While THEMIS lacks the spectral resolution of TES, apparent thermal inertia can still be determined (Fergason et al., 2006b), and the spatial resolution increase of THEMIS over TES can be used to find heterogeneous mixing at a spatial resolution an order of magnitude lower than in previous work (Putzig et al., 2014).

1.4. Opportunity Rover Traverse

Opportunity's mission duration has surpassed 5000 sols, (a sol is a Martian day), many more than its originally planned 90 sols. This 14-year journey has taken the rover across a diverse range of terrains and inferred paleoenvironments. *Opportunity* landed in Eagle crater within Meridiani Planum and spent over 50 sols exploring the area (Squyres et al., 2004). Endurance crater contained some outcrops of bedrock within the crater walls but also contained abundant sand deposits (Squyres et al., 2006), as well as rocky and sandy regions (~sol 88). Further along, *Opportunity* encountered an aeolian ripple which entrapped it for 40 sols (~sol 446). Both regions would have been prime candidates for testing of variability in apparent thermal inertia, but their areal extent may not be large enough to be resolved by THEMIS. However, *Opportunity* made long traverses through a series of "pergatoids," or ripples potentially capable of entrapping the rover, around sol 2250 (Arvidson et al., 2011). This ripple field is large enough to easily span several THEMIS pixels and therefore makes an initial prime candidate for study. Areas within this region (within the context of THEMIS detectability) are thermophysically homogenous due to aeolian sorting. Elsewhere within this region, the ripples that partially mantle the surrounding bedrock create a horizontal, checkerboard-style mixing, which provides an ideal opportunity to test the sensitivity of this method for identifying sub-pixel heterogeneity.

2. Hypothesis

Discrepancies between predawn apparent thermal inertia measurements have previously been attributed to inherent uncertainties in measurements or model assumption uncertainties (Fergason et al., 2006b). This previous approach differs from the model presented here. Fergason et al. 2006b refers only to variability between different measurements at similar times of day. The present model assumes a two-component mixture of thermal inertias which can yield variations in apparent thermal inertia over a diurnal cycle. Therefore, regions of only fine sand or only bedrock should exhibit constant, yet different, apparent thermal inertias throughout the course of a day, whereas a region with a mixture of bedrock and fine sand would exhibit variable apparent thermal inertias which trend towards the warmest component at any given time of day. This effect leads to two primary hypotheses:

Null Hypothesis: Any diurnal variability in THEMIS-derived apparent thermal inertia is inherent to the instrument or thermal model, or errors in the parameters used by the thermal model, and does not correlate with the physical surface properties of the region.

Alternative hypothesis: Diurnal variability in the THEMIS-derived apparent thermal inertia of a surface can indicate multi-component mixing of thermal inertias, which indicates sub-resolved variations in the physical surface properties of the region.

These hypotheses will first be examined through theoretical modeling before exploring the hypotheses using empirical data of a well-characterized region on the ground.

An additional alternative hypothesis to explain diurnal variations in apparent thermal inertia is the presence of *vertical* layering on a scale shorter than the diurnal skin depth of the surface, a phenomenon currently being investigated by Ahern and Rogers (2018). This work instead focuses on the effect of *lateral* (horizontal) sub-pixel checkerboard mixing in which the lateral scale of mixing is large compared to the horizontal length scale of diurnal heat transfer. Both types of two-component mixing are plausible for Mars, but one type may dominate over the other at specific sites due to local geologic circumstances. Since neither effect has been characterized fully up until this point, and because each are complex in their own right, it is more tractable to study them independently before considering their combined effect.

3. Methods

3.1. Theoretical Modeling

The theoretical model creates virtual THEMIS "data collections" based on the mixture of two theoretical input components (Figure 2) using lookup tables of varying thermal inertias and albedos. Because absolute thermal inertia is correlated directly to the physical surface characterization on Mars (Kieffer et al., 1977; Jakosky, 1986; Presley and Christensen, 1997; Fergason et al., 2006a), varying thermal inertia within the model has the same effect as varying the size of grains or surface component. Lookup tables must be created individually for any given location and solar longitude through the KRC program provided by Arizona State University, krc.mars.asu.edu (Kieffer, 2013). The input variables used for thermal inertia calculations are (Kieffer, 2013):

Thermal Inertia: The resistance of a material to change in temperature in the presence of a radiant heat source, typically the Sun

Conductivity: The rate at which heat is conducted through a specified material

Density: The amount of mass, or matter, contained within a specific volume

Specific Heat: The amount of energy required to raise the temperature of a material

Opacity: A measure of the impenetrability of the atmosphere to electromagnetic radiation

Albedo: The proportion of the incident light or radiation that is reflected by a surface

Emissivity: The ratio of the radiance from the surface to that radiated from a blackbody at the same temperature and wavelength.

Slope: Angle of incline of a surface above or below horizontal

Azimuth: Direction of slope as measured beginning from north and moving through east

L_s : The Mars-Sun angle, measured from the Northern Hemisphere spring equinox where $L_s=0$

Pressure: The pressure exerted by the weight of the atmosphere

Diurnal Surface Temperature: Variations in temperatures occurring throughout a day

For model testing, most inputs remain constant to constrain the model. A series of lookup tables were constructed with input parameters tailored to the *Opportunity* landing site. These tables expedited the process and prevented the time-consuming thermal model from needlessly running every time a temperature was needed for a given thermal inertia and albedo. Instead the model parsed a pre-calculated lookup table. The primary lookup table used for this model used fixed values for all input parameters except **thermal inertia** and **albedo,** which therefore yields an array of fixed **temperatures** for predawn and midday data collections.

The thermal inertia ranged from 12 to 2000 tiu, encompassing all observed thermal inertias on the Martian surface, and were incremented by 1-tiu each run for high resolution sampling. Any values lying between thermal inertia or albedo values were linearly interpolated. The albedos spanned typical Martian values of 0.01 to 0.20 in increments of 0.01. The KRC program, using every combination of these input values, applied a thermal model of the surface of Mars to estimate the surface temperature at predawn and midday. This created a lookup table with 39,780 lines consisting of the albedo, thermal inertia and two temperatures output by KRC. One temperature value was calculated at predawn hours (0400 Local Mean Solar Time, or LMST) and the other was taken during midday hours (1400 LMST).

An interpolation code was constructed for this project so this lookup table could be used "backwards," and the theoretical model could use the predawn and midday temperatures of a surface composed of any mixture of components to find corresponding apparent thermal inertia values. A flowchart (Figure 2.) also is provided to further illustrate the process. The THEMIS detector measures spectral radiance, which can be converted into temperature. However, temperature is an intrinsic property and therefore two temperatures cannot simply be averaged together. Thus, any temperatures from the lookup tables must be converted into radiance space, averaged, and then converted back to an apparent temperature for the mixed surface. To maintain consistency with current THEMIS processing methods, only band 9 radiances are used for calculating temperatures ($\lambda = 8.56\ \mu m$) (Kieffer, 2013). After converting the two predawn temperature values and the two midday temperatures values into radiance space, they can be averaged by slightly modifying the blackbody equation:

$$B_\lambda(\lambda, T) = \frac{2hc^2}{\lambda^5}\frac{1}{e^{\frac{hc}{\lambda k_b T_1}}-1}x + \frac{2hc^2}{\lambda^5}\frac{1}{e^{\frac{hc}{\lambda k_b T_2}}-1}(1-x). \quad [4]$$

In equation 4, h is the Planck constant, c is the speed of light, λ is the band 9 wavelength of THEMIS, k_B is the Boltzmann constant, T_1 is the temperature of component 1 in Kelvin, T_2 is the temperature of component 2 in Kelvin, x is the mixing percentage of component 1, and $(1 - x)$ is the mixing percentage of component 2. The two radiances emitted by components 1 and 2 were mixed in proportion to their abundances, and then "detected" by THEMIS. The mixed radiance was then converted back into temperature space through an inversion of the blackbody equation. This inversion was performed twice, once for a predawn measurement and once for a midday measurement. The two apparent

temperatures for the two times of day were then fed into the inverse thermal model to find two thermal inertias, one corresponding closest to the predawn apparent temperature of the mixed components and the other corresponding closest to the midday apparent temperature. Finally, these two thermal inertias were subtracted from one another to find the delta thermal inertia (ΔI). The 50% mixture gave the largest diurnal variation in thermal inertia and was therefore used for much of the model-based testing.

By using this model repeatedly, a grid of thermal inertias with a fine sampling resolution was analyzed against one another and plotted onto a 2D comparison plot, where the x- and y-axes are the possible thermal inertias of components 1 and 2 in the mixture, respectively, with values ranging the full width of the lookup table (12-2000 tiu). The values at each x and y position are the ΔI values of two mixed thermal inertias. These ΔI values were then compared to the published THEMIS uncertainty on the absolute values of the thermal inertia of 20% (Fergason et al., 2006b) (Figure 3). This 20% uncertainty likely is conservative because it only takes into consideration a single surface thermal inertia, rather than a mixture of multiple thermal inertias. It was derived from comparisons of thermal inertias all acquired at similar (pre-dawn) times of day, which is different from how the ΔI used here is derived. For comparison, two other values for the possible uncertainty on the absolute value of a thermal inertia (5% and 10%) were considered in Figure 3 in addition to the 20% uncertainty by calculating the limit of detectability for all uncertainty values and comparing it to the calculated change in thermal inertia:

$$\Delta I > \sqrt{(\delta_P I_P)^2 + (\delta_{\mathrm{M}} I_M)^2} \therefore detectable$$

$$\Delta I < \sqrt{(\delta_P I_P)^2 + (\delta_{\mathrm{M}} I_M)^2} \therefore not\ detectable. \quad [5]$$

Here δ represents the uncertainty (5%, 10%, and 20%) in the apparent thermal inertia, I, at predawn, P, and midday, M. Through this equation, the uncertainty in ΔI is calculated based on the uncertainty associated with the corresponding pre-dawn and mid-day thermal inertia measurements, and if that is smaller than the corresponding ΔI value, the ΔI value would be above the uncertainty and therefore detectable. Each uncertainty was tested against the ΔI and a limit of detectability was determined. As shown by Figure 3, a heterogeneous surface consisting of 50% dust and 50% boulders should be detectable even with the 20% uncertainty in absolute thermal inertia asserted in Fergason et al. (2006b). While this level of detectability for heterogeneous surfaces is certainly useful, empirical results presented below suggest the method proposed here is also sensitive to less extreme differences in mixing.

3.2. Site Selection

The *Opportunity* Mars rover landing site in Meridiani Planum was chosen as the primary location for this study as the rover has traversed over 45-km across a variety of terrains. Some of these terrains contain mixtures of both bedrock and sand (Figure 4) while others are primarily covered in sand (Figure 5). Regions that have a wide variety in the degree of surface heterogeneity (at the 100-m scale of a THEMIS pixel) make ideal candidates for searching for evidence of diurnal variability in apparent thermal inertia.

To further evaluate the utility of ΔI as a proxy for surface heterogeneity, images from *Opportunity's* hazard avoidance cameras (Hazcams) were inspected manually to assess the degree of heterogeneity and compared to ΔI values derived from THEMIS data for the same locations. The front Hazcam images were selected for this evaluation, rather than the

microscopic imager (MI) images. Images from the hazard avoidance cameras were chosen to keep a constant viewing angle to maintain consistency between rover locations and because these images cover areas much closer to the extent of a THEMIS pixel than an MI image. Also, Hazcam can resolve larger components of the surface mixtures found at Meridiani Planum, and the grain size of the smaller components visible in Hazcam images were "spot checked" using the MI and Mini-Thermal Emission Spectrometer (MiniTES) where available (Fergason et al., 2006a).

The High Resolution Imaging Science Experiment (HiRISE) has a resolution of 25-32-cm/pixel (McEwen et al., 2007). This resolution is insufficient to directly determine surface mixing at the resolution of this ΔI method. However, there are characteristic differences between the albedos of sand and bedrock specific to the materials encountered along the *Opportunity* traverse at Meridiani Planum that allowed use of albedo to determine the proportions of sand and bedrock at the THEMIS pixel scale from HiRISE images. Therefore, HiRISE images were used as a proof-of-concept for this thermal analysis by analyzing the degree of heterogeneity over the *Opportunity* traverse. The combination of available ground observations and the simple relationship between albedo and surface component at this site provided an excellent means of validating the method proposed here. If validated, this method can be used globally in regions with no ground-based coverage or different relationship between albedo and surface component in HiRISE images.

3.3. Data Collection

Comparing THEMIS measurements between two separate scenes carries a high degree of uncertainty (Fergason et al., 2006b). To mitigate this uncertainty, three criteria were

given special consideration during image selection: Mars Year, Solar Longitude, and Image Rating. Images were required to have been acquired by THEMIS during the same Mars year, and as close to the same solar longitude as possible. This was to minimize time-variable contributions to the uncertainty, such as the amount of dust loading in the atmosphere. THEMIS complete repeat coverage occurs approximately every 30 days near the equator (Christensen et al., 2004). This is a maximum time for repeat coverage; images that overlap at predawn and midday are more common. Furthermore, coverage repeat at the poles is faster, so midday and predawn image pairs are temporally close, and images were selected to maximize this temporal proximity. Image quality also plays a major factor in image processing. THEMIS images are rated based on exposure, missing lines, instrument noise, and atmospheric features. Image ratings range from 1 to 7, with 7 being extremely rare, pristine quality, 3 to 6 the generally acceptable range for image quality, and 1 to 2 being low quality images unsuitable for research purposes. For this research, only images with an image rating of 4 and above were used. The ΔI method relies on subtle diurnal shifts in apparent thermal inertia, and using high quality images maximizes the chances of detecting these shifts.

Two THEMIS infrared images (image numbers I53125002 and I53343006) were used for the analysis of the Meridiani Planum site. Both images overlap over Endeavor crater and the remainder of the *Opportunity* traverse. They are separated by only 8° of solar longitude (one month is 30°) and both were taken in the Martian spring. Image I53125002 has an image quality of 4 and I53343006 has an image quality of 5.

3.4. Data Processing with MARSTHERM

The THEMIS images were processed through MARSTHERM (Putzig et al., 2013), a model created by the Southwest Research Institute. While KRC is a variation on the original thermal model crafted by Hugh Keiffer in FORTRAN (Kieffer et al., 1977), MARSTHERM uses an enhanced version of the thermal inertia derivation algorithm developed by Mellon et al. (2000). MARSTHERM has a web-based interface which simplifies the processing of THEMIS images compared to using KRC. Fergason (2006b) showed that "any differences between the thermal models does not significantly contribute to differences between derived thermal inertia values".

Image outputs from MARSTHERM consist of several products, all of which are map projected and cropped to user defined coordinates: a processed radiance image of the region of interest, an apparent thermal inertia image, and a quality factor image. The MARSTHERM quality factor (0-5) is distinct from the individual THEMIS image rating in that: A) it is assessed on a per-pixel basis rather than based on the entire image, and B) the quality factor of MARSTHERM is based on interpolation value accuracy and varies from pixel to pixel, whereas the THEMIS image rating is a subjective assessment of image quality based on conditions such as exposure, noise, any missing lines, and atmospheric features. It should be noted that the sense of these two quality indicators are opposite each other; low MARSTHERM quality factors (0-good to 3-useable) and high THEMIS image ratings (3-useable to 7-good) are desirable for analysis (Putzig et al., 2013).

3.5. Data Processing with ENVI

The MARSTHERM-processed images (based on images I53125002 and I53343006 as input) were taken into ENVI (ENvironment for Visualizing Images) for further processing. These images were masked to remove any pixels of a quality factor of 4 or 5. The two masks were compared and pixels that were masked from one image due to poor quality factor also were masked from the other image. This way only pixels with thermal inertia values with quality factors of 0-3 were used to produce the ΔI image. MARSTHERM produces image products that have been georectified using SPICE kernels and cropped to a user-set longitude and latitude. The ground resolution of the two images were the same (100-m/pixel), so the images overlaid each other to the pixel and were easily subtracted from one another easily. A manual "flicker" between images was used prior to the subtraction to verify the positioning of the images, but no correction was needed. A slight, approximately 0.1-degree grid pattern is visible across processed images which is caused by the memory limitations in MARSTHERM.

3.6. Data Processing with ArcGIS

ArcGIS is used to visualize the final subtraction step in the diurnal thermal inertia comparison with orbital images and the rover traverse. However, while the thermal inertia images were cropped and co-rectified, the resultant ΔI image was not georectified. Tie points registered the ΔI image to the CTX and HiRISE basemap of the *Opportunity* rover traverse location (Parker et al., 2012). A color ramp was added to the basemap to clearly show variations in ΔI (Figure 6). Low ΔI values therefore correspond to more homogeneous surface mixtures, while higher ΔI values should correspond to more

heterogeneous surface mixtures. The georeferenced traverse of *Opportunity* then was overlain to visualize the path and to select regions of interest along it for further investigation. Locations of interest were selected from specific pixels that have very low or very high ΔI values. Regions with high topographic slope (>15°) were avoided to mitigate against thermoclinometric effects, which can significantly influence the apparent thermal inertia values inferred from midday THEMIS images (Fergason et al., 2006b). While the model does include a slope correction, thermoclinometric effects on sloped surfaces still may yield spurious thermal inertia values, especially in the midday images. This is due to the MOLA data used for the elevation map. MARSTHERM uses an elevation map of 20 pixels per degree, and elevation values are interpolated linearly. As the DEM used to get slope values has a lower resolution than the resolution of the THEMIS data, high sloped regions were avoided for this study.

Selected regions of interest were linked to a specific sol number for the rover and front Hazcam images were acquired for those sols. Regions where the rover stayed for multiple sols used the images from the first sol in that location. Images throughout the traverse were selected by choosing a sol located around 100-m from the previous image location. If that sol did not have a Hazcam image, the next sol with a Hazcam image was selected. For the study location, 64 images were selected for manual evaluation of the degree of surface heterogeneity by independent reviewers. Each Hazcam image field of view is less than 50-m in front of the rover and images are acquired during every drive the rover completes. Therefore, while Hazcam images do not have the pixel resolution necessary to differentiate varying sand sizes, they are ideal for differentiating sand and bedrock over an area of a size approaching that of a THEMIS pixel.

Volunteers (n=12) were selected to evaluate the degree of surface heterogeneity of the selected 64 images taken along the traverse. First, the volunteers scanned through the images without rating to become accustomed to the scenes, then rated each image from 1 (very homogeneous) to 5 (very heterogeneous) based on 5 sample images at each degree of heterogeneity. After rating once, the volunteers began again so the first images were rated in a similar manner to the final images. For an assessment of surface heterogeneity, only the second set of ratings was used from each volunteer. The results then were averaged for each location. Image ratings for each location all had standard deviations of less than 1.5, so more reviewers were deemed unnecessary. Each rating for the images then was then logged to the correct sol in the *Opportunity* traverse within ArcGIS and compared to the value of the corresponding pixel in the ΔI image (Figure 7). Here, darker green circles indicated a larger degree of surface heterogeneity and therefore should correspond to an increase in ΔI if the alternative hypothesis stated in Section 2 is true.

3.7 Processing HiRISE Images

Three HiRISE stamps were selected for this region to fully cover the portion of *Opportunity's* traverse being investigated (ESP_012820_1780, ESP_020758_1780, and PSP_009141_1780). Images ranged in scale from 26.9- to 29.6-cm/pixel, and each were taken at 15:27 $\pm$ 00:05 LMST. As seen in Figure 5, the approximate proportions of fines vs. bedrock along the *Opportunity* traverse easily can be assessed in rover-based images because the lighter-toned bedrock contrasts heavily with the darker-toned sand. As these happen to be the two dominant size fractions along the traverse, a threshold was applied to the HiRISE images of the region to separate each image into dark pixels representing fine

sand, and light pixels representing bedrock, and this bimodal image was used to assess the degree of lateral checkerboard mixing at the 100-m scale of THEMIS observations.

However, the HiRISE pixel radiance values for each of these two units within the images were not uniform throughout the images. This was due to an overall gradient in gain the flat field correction was not able to correct which likely would not have been seen had the data not had a threshold applied. Reducing the data down to two unique values caused this gradient to become apparent, so a correction for this gradient was necessary. Once the 3 HiRISE stamps were combined into one mosaic, the *Opportunity* traverse was overlain. The section of the HiRISE mosaic surrounding the traverse was broken into subsections of 1-km x 2-km. This size was picked as it was below the scale of the gain drift. Each subsection overlapped the previous subsection by approximately 10%, so they could be mosaicked together later to verify consistency of the sand/bedrock identification. A threshold was applied to each subsection in such a way as to separate the lighter toned material from the darker toned material (Figure 8).

The thresholded subsections were mosaicked together, and the resultant HiRISE threshold map was then imported into ArcGIS and registered to the georectified HiRISE basemap. This HiRISE threshold is designed to calculate the percentage of bedrock and sand that would be present in any given THEMIS pixel. To do this, square 100-m buffers were created around each stop in the *Opportunity* traverse. This buffer served as an analog for a THEMIS pixel, and through a program written by ArcGIS user clarksu (2012), the number of light and dark pixels within each 100-m square buffer in the underlying HiRISE threshold was tallied, and a percentage of exposed bedrock was calculated. These data

were then compared to the average user submitted degree of heterogeneity and the map of ΔI values (Figure 9) using the rover position at each sol, the center of each 100-m square.

4. Results

4.1. Theoretical Model

The results of the theoretical study were plotted on a 2D comparison graph in three increments of component mixing under ideal conditions: a 50% mixture of two components (Figure 3a), a 25% mixture of two components (Figure 3b), and a "0% mixture" (homogeneous surface) as a control. A detection limit estimated based on the uncertainty in absolute thermal inertia provided by Fergason et al. (2006b) was calculated and plotted on each graph. The control test for the homogeneous surface successfully resulted in a ΔI of 0 for all pixels. As this model used the same absolute thermal inertia for the two components being mixed, when "averaged" the pixel exhibited the same apparent thermal inertia at predawn and midday indicating the model performed nominally. The second verification of the model was the 25:75 ratio image, which calculated most heterogeneous surfaces would not be detectable at a 20% uncertainty. In fact, only bedrock/dust mixtures yielded ΔI values in excess of this limit, with an apparent thermal inertia difference of 100-110-tiu between predawn and midday.

The final theoretical feasibility check for the method utilized a 50:50 mixture of component 1 to component 2 and yielded ΔI values up to 225-tiu, over 100-tiu greater than the 25:75 mixture. Even in a 50:50 mixture, plot contours corresponding to 20% uncertainty suggest any surface heterogeneities less extreme than a mixture of bedrock and dust, gravel-dust or cobble-dust would not be detectable via THEMIS.

4.2. In-situ Analysis

Initially, two locations were chosen as places to make a qualitative "spot check" comparison of Δ*I* with what was seen on the ground by *Opportunity*. The first location, visited on sol 2246 of the mission, was chosen on flat ground with a homogeneous (as defined above) surface (Figure 5), as dust and sand mixtures are indistinguishable and no significant percentage of the area contained bedrock. The other location, from sol 2376, was chosen for its heterogeneous surface consisting of bedrock outcroppings and sand (Figure 4). The homogenous location had a *ΔI* value of 4-tiu, whereas the heterogeneous location had a *ΔI* of 123-tiu. After the spot-check method, the mixtures of the corresponding surfaces were plotted onto the theoretical 50% mixing plot in Figure 3a. This Δ*I* value of 4-tiu corresponds to a homogeneous surface, and using knowledge gained from *in-situ* observations and by estimating grain size from predawn THEMIS images it was concluded the surface consists of fine sand. The value of 123-tiu corresponds to a mixed thermal inertia surface, which here using *in-situ* observations can be refined to a 50:50 mixture of fine sand and bedrock. The Δ*I* values were similar to the modeled results. The *in-situ* analysis provided by the volunteers was also compared to the corresponding Δ*I* for each location. The correlation between Δ*I* and user-submitted degree of heterogeneity was plotted on a series of histograms intended to reveal any correlation between these values, hereafter referred to as a "correlation histogram" (Figure 10a).

4.3. Comparison Between ΔI Values and Masked HiRISE image

The analysis of the 100-m buffered points along the MER traverse yielded similar, but significantly more results than the manual identification performed by the volunteers.

Values for the percentage of bedrock exposed ranged from 0% to 54%. The same portion of *Opportunity's* traverse, between sols 2395 and 2594, contained the highest values of heterogeneity. Furthermore, as the mixing ratio approached 50:50, a similar increase was seen in the correlation histogram plot for ΔI values (Figure 10b).

5. Discussion

The analysis performed by the volunteers appears to reveal a correlation between their evaluation of heterogeneity and in ΔI, but this correlation is not as strong as the correlation seen in the HiRISE analysis. Perhaps this is because the Hazcams onboard *Opportunity* fail to resolve surface features farther than 50 m away. This resolution hinderance, plus the single orientation per sol from the front of the rover limits the observation window to a small subset of a 100-m THEMIS pixel. For a better representation of each THEMIS pixel, multiple Hazcam images within each THEMIS pixel could be analyzed over more of the *Opportunity* traverse. However, sufficient Hazcam analysis over the amount of traverse examined here would require that thousands of images be checked by volunteers.

Luckily, within this region at Meridiani Planum albedo differences between sand and bedrock were distinct enough for percentages of these two components to be extracted from HiRISE images. While this HiRISE method may work well in Meridiani, other regions on Mars may not have such a strong correlation between albedo and the distribution of sand, and even if such a correlation exists elsewhere, the albedo differences may not be stark enough to separate them. The use of the same 100-m square buffer for HiRISE percent mixing was chosen to be at the same size as a THEMIS pixel for direct comparison. When plotted on the comparison histogram, a distinct trend is seen where pixels of higher HiRISE percent mixing correlate with values of lower ΔI. As the degree of heterogeneity increases, the range of ΔI values also increases, to the point where a 50% mixture, or a maximally heterogeneous surface, corresponds to ΔI values of 100-tiu to more than 120-tiu. Some variability was seen on this histogram where lower percent mixing correlated with increases in ΔI and higher percent mixing correlated to decreases. However, these

were uncommon, and may be caused by illuminated ripple crests (Figure 8). This is a limitation of the thresholding performed and could lead to an apparent increase in percent mixing over homogeneous surfaces.

By analyzing the first "spot-check" location on sols 2246 and plotting it on the theoretical 50% mixing plot (Figure 3a), it was found that the ΔI of 4-tiu is well below the limit of detectability associated with 20% uncertainty between scenes, as expected for a site with a homogeneous surface. However, sol 2377, which was located in a region of high heterogeneity, corresponds with a ΔI value of 123-tiu, and when plot on the theoretical plot this ΔI value lies just above the limit of detectability for a 20% uncertainty. The higher than expected sensitivity of the method may suggest that previous estimates of the 20% uncertainty in THEMIS derived thermal inertia values may be unnecessarily pessimistic, but it could also be caused by the high-grading of the data. These data were selected specifically for a single season and taken within only a few weeks. Perhaps the rigorous selection process for these images reduced some of the uncertainty suggested by Fergason et al. (2006b). The correlation of high heterogeneity with a high ΔI value of both the spot-check locations and the correlation plot in Figure 10b indicates surfaces of fine sand and bedrock can be detected through diurnal THEMIS thermal inertia comparisons. This correlation allows for an acceptance of the alternative hypothesis.

6. Summary

A new technique has been evaluated for remotely mapping surface heterogeneity on the Martian surface using diurnal variations in apparent thermal inertia values derived from THEMIS infrared image pairs acquired in the pre-dawn and mid-day hours. Through inverse and forward modeling, variations in calculated thermal inertia caused by surface heterogeneity should be detectable for laterally-mixed surfaces with extreme differences in thermal inertia variability (i.e., dust mixed with bedrock). These results were then tested at Meridiani Planum, the location of the landing site and traverse of the *Opportunity* rover, by looking for variations in surface heterogeneity in front Hazcam images and comparing this to a map of ΔI, the difference in apparent thermal inertia inferred from midday and predawn THEMIS measurements. To further test this method, surface heterogeneity was evaluated with high-resolution HiRISE images for regions of high-albedo bedrock and low-albedo sand to compare to the ΔI map.

Previous apparent thermal inertia estimates had assumed a single apparent thermal inertia for each pixel. This new method can be used to distinguish surfaces that have relatively uniform surfaces from those that have mixed surfaces if the grain sizes are disparate enough and may show that previous estimates for uncertainty for THEMIS data were higher than the true value.

Currently, images from the High-Resolution Imaging Science Experiment (HiRISE) cover only ~2.4% of the Martian surface. By contrast, THEMIS day and night infrared coverage is nearly global. This method can be a rapid and practical analytical technique to determine the degree of surface heterogeneity for future landing sites.

Furthermore, knowing the degree of surface heterogeneity can aid in geomorphologic studies. Because current interpretations of thermophysical measurements are based on the assumption that surfaces are composed of a single thermal inertia, the ability to determine whether a given area contains a distribution of multiple components or simply a single component will be of use to geomorphologists and engineers studying Mars' past geologic history and potential future landing sites. Any research which has used THEMIS for physical surface characteristic estimations could be reanalyzed for regions with diurnal imagery to refine the degree of surface mixing. For instance, crater ejecta studies could benefit due to the abundance of surface size components within crater ejecta; ancient fluvial channel systems could be examined to determine the sorting along the channel bed; and dune fields can be analyzed for variations in sorting. Identification of many geologic processes can be aided by knowledge of the resultant variations in surface characteristics, so this method can be another tool in a remote sensing specialist's toolbox for identifying these processes from thermal data.

One caveat however is that midday thermal inertia maps are used, which still are affected by preferential heating, even when built-in slope corrections are used. Therefore, high sloped ($>15°$) regions should be avoided or examined with careful consideration. The terrain along *Opportunity's* traverse is primarily flat, and therefore slopes above ~15 degrees were not examined in the course of this study, avoiding the aforementioned slope heating issues.

As the variations in THEMIS apparent thermal inertia between predawn and midday images are shown to correlate to regions of surface heterogeneity, the alternative hypothesis can be accepted: variability in the THEMIS-derived apparent thermal inertia of

a surface over a diurnal cycle indicates multi-component mixing of thermal inertias. This indicates sub-resolved variations in the physical surface properties of the region. These variations can be detected in data taken by the THEMIS instrument if the components are sufficiently different from each other and the different sizes are present in large enough proportions. This method of observing differences in diurnal thermal inertia pairs is the preferred method for determining the degree of surface heterogeneity as HiRISE does not have a global dataset, cannot directly observe components smaller than large cobbles, and other regions may not have component mixtures which correlate with albedo as neatly as those in Meridiani Planum do. The THEMIS ΔI map can discern surface heterogeneity detectable by HiRISE within Meridiani Planum, and hopefully can be another tool in the geomorphologists toolkit to identify horizontal surface heterogeneity across the rest of the planet.

List of References

Ahern, A.A., Rogers, A.D., 2018. Contraining the Thermal Inertia of Martian Bedrock Exposures Using Overlapping THEMIS Observations, in: Lunar and Planetary Science Conference. Lunar an Planetary Science Conference XLIX, Houston, TX, p. 2.

Arvidson, R.E., Ashley, J.W., Bell, J.F., Chojnacki, M., Cohen, J., Economou, T.E., Farrand, W.H., Fergason, R., Fleischer, I., Geissler, P., Gellert, R., Golombek, M.P., Grotzinger, J.P., Guinness, E.A., Haberle, R.M., Herkenhoff, K.E., Herman, J.A., Iagnemma, K.D., Jolliff, B.L., Johnson, J.R., Klingelhöfer, G., Knoll, A.H., Knudson, A.T., Li, R., McLennan, S.M., Mittlefehldt, D.W., Morris, R. V., Parker, T.J., Rice, M.S., Schröder, C., Soderblom, L.A., Squyres, S.W., Sullivan, R.J., Wolff, M.J., 2011. Opportunity Mars Rover mission: Overview and selected results from Purgatory ripple to traverses to Endeavour Crater. J. Geophys. Res. 116, E00F15. https://doi.org/10.1029/2010JE003746

Christensen, P.R., Bandfield, J.L., Hamilton, V.E., Ruff, S.W., Kieffer, H.H., Titus, T.N., Malin, M.C., Morris, R. V., Lane, M.D., Clark, R.L., Jakosky, B.M., Mellon, M.T., Pearl, J.C., Conrath, B.J., Smith, M.D., Clancy, R.T., Kuzmin, R.O., Roush, T., Mehall, G.L., Gorelick, N., Bender, K., Murray, K., Dason, S., Greene, E., Silverman, S., Greenfield, M., 2001. Mars Global Surveyor Thermal Emission Spectrometer experiment: Investigation description and surface science results. J. Geophys. Res. Planets 106, 23823–23871. https://doi.org/10.1029/2000JE001370

Christensen, P.R., Jakosky, B.M., Kieffer, H.H., Malin, M.C., Jr, H.Y.M., Nealson, K., Mehall, G.L., Silverman, S.H., Ferry, S., Caplinger, M., Ravine, M., 2004. The Thermal Emission Imaging System (THEMIS) for the Mars 2001 Odyssey Mission, in: 2001 Mars Odyssey. Springer Netherlands, Dordrecht, pp. 85–130. https://doi.org/10.1007/978-0-306-

48600-5_3

Clarksu, 2012. ZonalStatsOverlappingPolys. https://www.arcgis.com/home/item.html?id=b859b33c616a47d2b99b5e133942db02.

Eibl, M., Fedo, C., E Friday, M., McSween Jr., H.Y., 2015. The Accuracy of 2D Rover Imagery for Representing 3D Sedimentary Textures of Basaltic Mars Analog Sediment.

Fergason, R.L., Christensen, P.R., Bell, J.F., Golombek, M.P., Herkenhoff, K.E., Kieffer, H.H., 2006a. Physical properties of the Mars Exploration Rover landing sites as inferred from Mini-TES-derived thermal inertia. J. Geophys. Res. Planets 111, n/a-n/a. https://doi.org/10.1029/2005JE002583

Fergason, R.L., Christensen, P.R., Kieffer, H.H., 2006b. High-resolution thermal inertia derived from the Thermal Emission Imaging System (THEMIS): Thermal model and applications. J. Geophys. Res. Planets 111, n/a-n/a. https://doi.org/10.1029/2006JE002735

Folk, R.L., 1974. Petrology of Sedimentary Rocks: The University of Texas, Geology 370 K, 383 L, 383 M., Web. ed. University of Texas at Austin.

Grant, J.A., Golombek, M.P., Grotzinger, J.P., Wilson, S.A., Watkins, M.M., Vasavada, A.R., Griffes, J.L., Parker, T.J., 2011. The science process for selecting the landing site for the 2011 Mars Science Laboratory. Planet. Space Sci. 59, 1114–1127. https://doi.org/10.1016/j.pss.2010.06.016

Grant, J.A., Golombek, M.P., Parker, T.J., Crisp, J.A., Squyres, S.W., Weitz, C.M., 2004. Selecting landing sites for the 2003 Mars Exploration Rovers. Planet. Space Sci. 52, 11–21.

https://doi.org/10.1016/j.pss.2003.08.011

Iversen, J.D., Pollack, J.B., Greeley, R., White, B.R., 1976. Saltation Threshold on Mars: the Effect of Interparticle Force, Surface Roughness, and Low Atmospheric Density. Icarus 29, 381–393. https://doi.org/10.1016/0019-1035(76)90140-8

Jakosky, B.M., 1986. On the thermal properties of Martian fines. Icarus 66, 117–124. https://doi.org/10.1016/0019-1035(86)90011-4

Kieffer, H.H., 2013. Thermal model for analysis of Mars infrared mapping. J. Geophys. Res. Planets 118, 451–470. https://doi.org/10.1029/2012JE004164

Kieffer, H.H., Martin, T.Z., Peterfreund, A.R., Jakosky, B.M., Miner, E.D., Palluconi, F.D., 1977. Thermal and albedo mapping of Mars during the Viking primary mission. J. Geophys. Res. 82, 4249–4291. https://doi.org/10.1029/JS082i028p04249

McEwen, A.S., Eliason, E.M., Bergstrom, J.W., Bridges, N.T., Hansen, C.J., Delamere, W.A., Grant, J.A., Gulick, V.C., Herkenhoff, K.E., Keszthelyi, L., Kirk, R.L., Mellon, M.T., Squyres, S.W., Thomas, N., Weitz, C.M., 2007. Mars Reconnaissance Orbiter's High Resolution Imaging Science Experiment (HiRISE). J. Geophys. Res. 112, E05S02. https://doi.org/10.1029/2005JE002605

Mellon, M.T., Jakosky, B.M., Kieffer, H.H., Christensen, P.R., 2000. High-Resolution Thermal Inertia Mapping from the Mars Global Surveyor Thermal Emission Spectrometer. Icarus 148, 437–455. https://doi.org/http://dx.doi.org/10.1006/icar.2000.6503

Parker, T.J., Calef, F.J., Golombek, M.P., Hare, T.M., 2012. High-Resolution Basemaps for Localization, Mission Planning, and Geologic Mapping at Meridiani Planum and Gale Crater, in: Lunar and Planetary Science Conference. Lunar an Planetary Science

Conference XLIII, Houston, TX, p. 2535.

Presley, M.A., Christensen, P.R., 1997. Thermal conductivity measurements of particulate materials 2. Results. J. Geophys. Res. Planets 102, 6551–6566. https://doi.org/10.1029/96JE03303

Putzig, N.E., 2006. Thermal inertia and surface heterogeneity on Mars. University of Colorado.

Putzig, N.E., Barratt, E.M., Mellon, M.T., Michaels, T.I., 2013. MARSTHERM: A Web-based System Providing Thermophysical Analysis Tools for Mars Research, in: AGU Fall Meeting Abstracts. AMER GEOPHYSICAL UNION, San Francisco, p. 1.

Putzig, N.E., Mellon, M.T., 2007a. Apparent thermal inertia and the surface heterogeneity of Mars. Icarus 191, 68–94. https://doi.org/10.1016/j.icarus.2007.05.013

Putzig, N.E., Mellon, M.T., 2007b. Effects of Surface Heterogeneity on the Apparent Thermal Inertia of Mars. Lunar an Planetary Science Conference XXXVII, p. 2.

Putzig, N.E., Mellon, M.T., Herkenhoff, K.E., Phillips, R.J., Davis, B.J., Ewer, K.J., Bowers, L.M., 2014. Thermal behavior and ice-table depth within the north polar erg of Mars. Icarus 230, 64–76. https://doi.org/10.1016/j.icarus.2013.07.010

Squyres, S.W., Arvidson, R.E., Bell, J.F., Bruckner, J., Cabrol, N.A., Calvin, W.M., Carr, M.H., Christensen, P.R., Clark, B.C., Crumpler, L.A., Des Marais, D.J., D'Uston, C., Economou, T.E., Farmer, J., Farrand, W.H., Folkner, W., Golombek, M.P., Gorevan, S., Grant, J.A., Greeley, R., Grotzinger, J.P., Haskin, L., Herkenhoff, K.E., Hviid, S., Johnson, J.R., Klingelhöfer, G., Knoll, A.H., Landis, G., Lemmon, M.T., Li, R., Madsen, M.B., Malin, M.C., McLennan, S.M., McSween, H.Y., Ming, D.W., Moersch, J., Morris, R. V., Parker, T.J., Rice,

J.W., Richter, L., Rieder, R., Sims, M., Smith, M., Smith, P., Soderblom, L.A., Sullivan, R.J., Wanke, H., Wdowiak, T., Wolff, M.J., Yen, A.S., 2004. The Opportunity Rover's Athena Science Investigation at Meridiani Planum, Mars. Science (80-.). 306, 1698–1703. https://doi.org/10.1126/science.1106171

Squyres, S.W., Arvidson, R.E., Bollen, D., Bell, J.F., Brückner, J., Cabrol, N.A., Calvin, W.M., Carr, M.H., Christensen, P.R., Clark, B.C., Crumpler, L., Des Marais, D.J., D'Uston, C., Economou, T., Farmer, J., Farrand, W.H., Folkner, W., Gellert, R., Glotch, T.D., Golombek, M., Gorevan, S., Grant, J.A., Greeley, R., Grotzinger, J., Herkenhoff, K.E., Hviid, S., Johnson, J.R., Klingelhöfer, G., Knoll, A.H., Landis, G., Lemmon, M., Li, R., Madsen, M.B., Malin, M.C., McLennan, S.M., McSween, H.Y., Ming, D.W., Moersch, J., Morris, R. V., Parker, T., Rice, J.W., Richter, L., Rieder, R., Schröder, C., Sims, M., Smith, M., Smith, P., Soderblom, L.A., Sullivan, R., Tosca, N.J., Wänke, H., Wdowiak, T., Wolff, M., Yen, A., 2006. Overview of the Opportunity Mars Exploration Rover Mission to Meridiani Planum: Eagle Crater to Purgatory Ripple. J. Geophys. Res. Planets 111, n/a-n/a. https://doi.org/10.1029/2006JE002771

Appendices

Appendix A: Figures

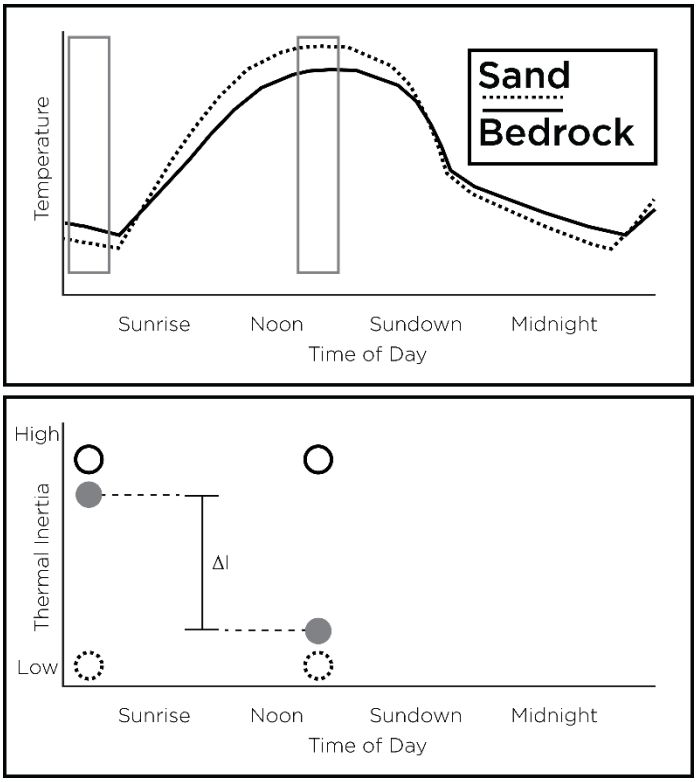

Figure 1. A schematic diagram showing the variability between predawn and midday observations of a mixed particle surface. The dashed line illustrates a diurnal thermal curve for a pixel consisting of 100% sand, while the solid line represents a similar diurnal thermal curve for a pixel of 100% bedrock. If a pixel lies on the boundary between the two, creating a 50:50 mixture (gray) of each, the resultant pixel, when measured will be offset towards the curve associated with the warmest particle size. The difference between calculated thermal inertia at predawn and midday is the change in thermal inertia (ΔI). This change is zero for pixels associated with homogeneous surfaces (solid and dashed circles) but nonzero for heterogeneous surfaces (gray circles).

Figure 2. Flowchart illustrating thermal inertia model for two particles with thermal inertias of 100 and 1500. The albedo and thermal inertia of two hypothetical surfaces are input into the model and matched with corresponding temperatures for each. Dashed borders are used to aid in the identification of different surfaces. The two midday temperatures and two predawn temperatures are converted into radiance space and each mixed linearly by observation time. The two combined radiances are then converted back to apparent temperatures by an inversion of the blackbody equation. These two temperatures are then input back into the original lookup table with no prior knowledge of the original temperatures or thermal inertias used to find midday and predawn apparent thermal inertias. The two new thermal inertias are then subtracted from one another to find the ΔI. Example values are listed to the right.

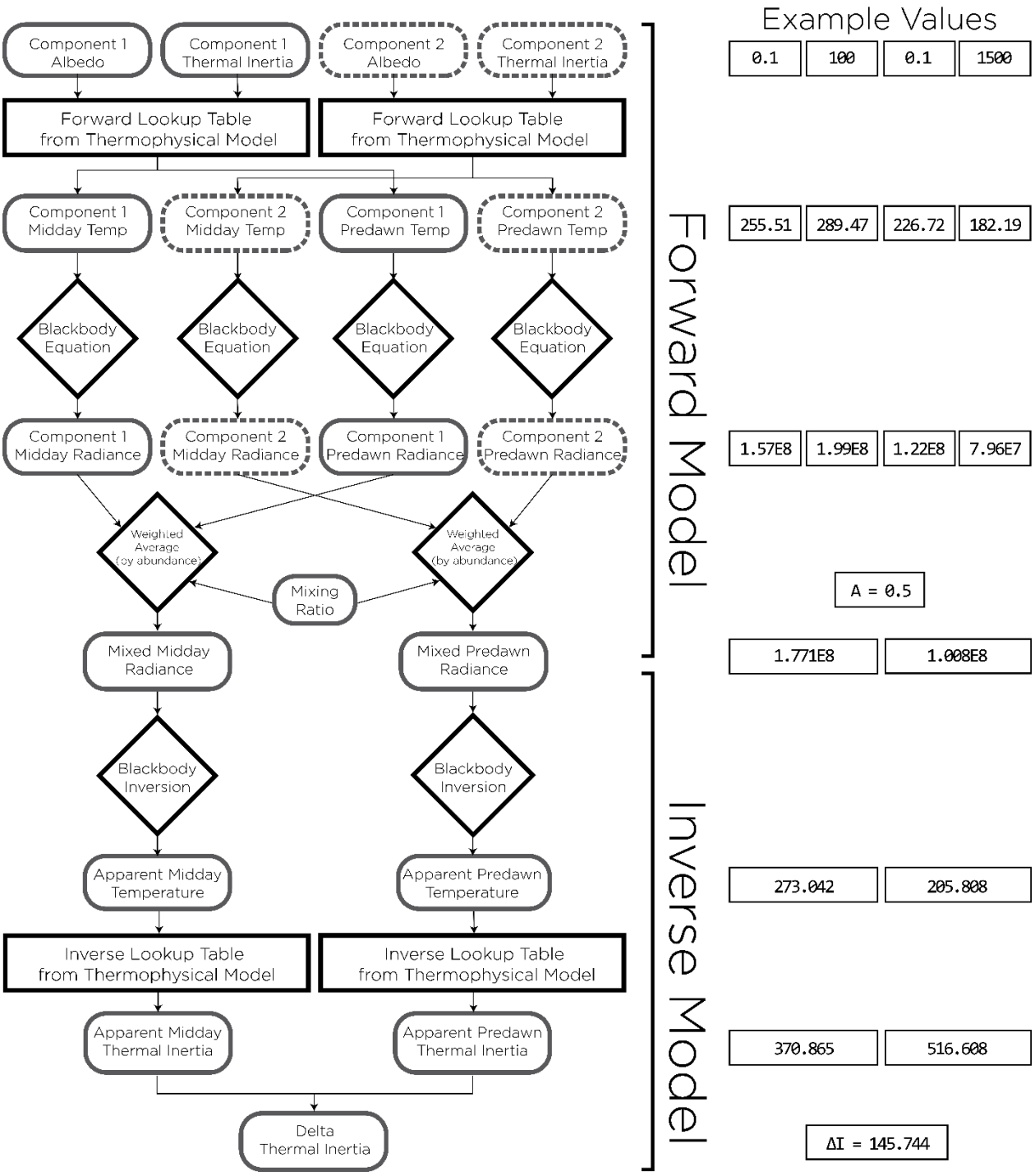
Example Values
Component 1 Albedo
Component 1 Thermal Inertia
Component 2 Albedo
Component 2 Thermal Inertia
0.1
100
0.1
1500
Forward Lookup Table from Thermophysical Model
Forward Lookup Table from Thermophysical Model
Component 1 Midday Temp
Component 2 Midday Temp
Component 1 Predawn Temp
Component 2 Predawn Temp
255.51
289.47
226.72
182.19
Blackbody Equation
Blackbody Equation
Blackbody Equation
Blackbody Equation
Component 1 Midday Radiance
Component 2 Midday Radiance
Component 1 Predawn Radiance
Component 2 Predawn Radiance
1.57E8
1.99E8
1.22E8
7.96E7
Weighted Average (by abundance)
Weighted Average (by abundance)
Mixing Ratio
A = 0.5
Mixed Midday Radiance
Mixed Predawn Radiance
1.771E8
1.008E8
Blackbody Inversion
Blackbody Inversion
Apparent Midday Temperature
Apparent Predawn Temperature
273.042
205.808
Inverse Lookup Table from Thermophysical Model
Inverse Lookup Table from Thermophysical Model
Apparent Midday Thermal Inertia
Apparent Predawn Thermal Inertia
370.865
516.608
Delta Thermal Inertia
ΔI = 145.744
Forward Model
Inverse Model

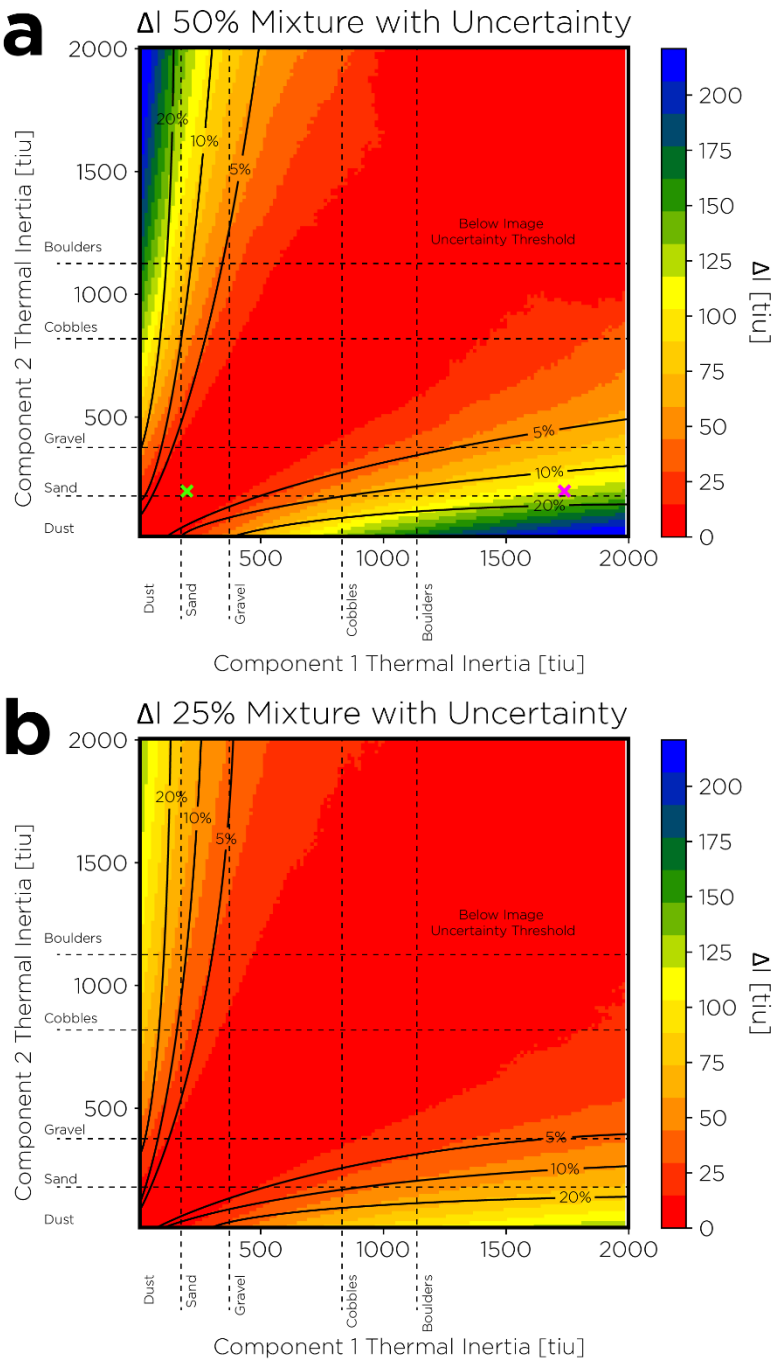

Figure 3. Theoretical mixing plots which take an either 50% (a) or 25% (b) amount of Particle A mixed with Particle B and calculate a corresponding ΔI that would be observed by THEMIS under ideal conditions. Lines indicate the limit of uncertainty in THEMIS measurements between scenes, the 20% value quoted by Fergason et al. (2006b). The two Xs in a represent ΔI values for sols 2246 (green) and 2377 (pink).

Figure 4. Pancam taken on sol 2376 by the Opportunity rover, and an example of a relatively heterogeneous surface (sand/bedrock).

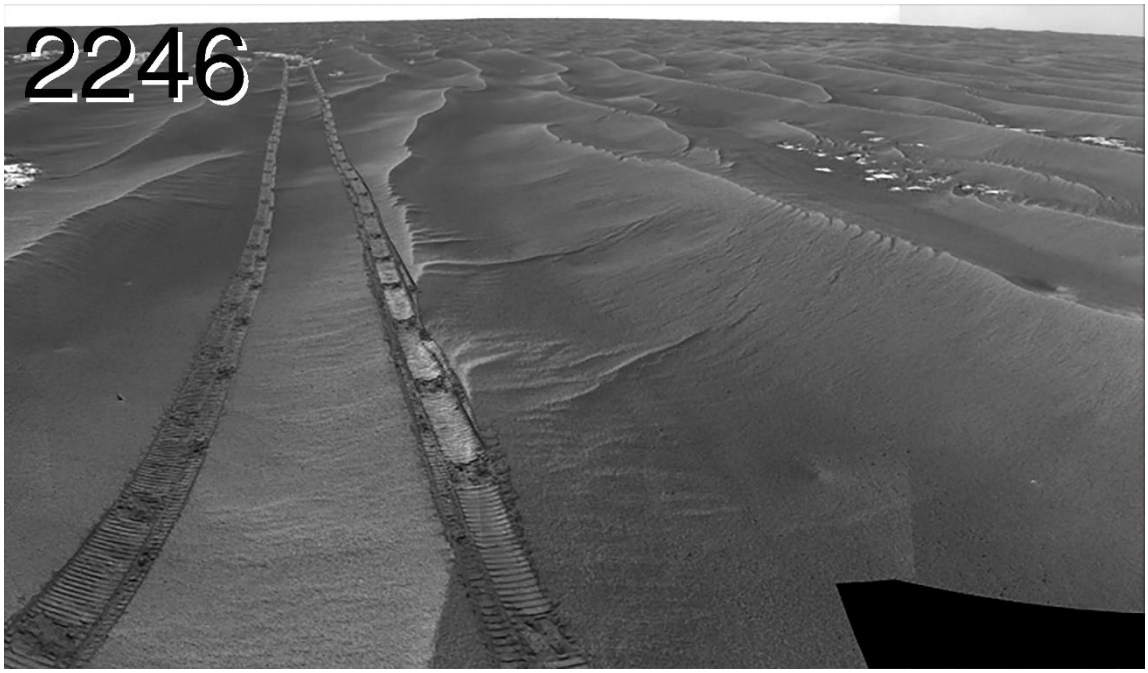

Figure 5. Pancam from sol 2246, and an example of relatively homogeneous surface (sand). Rover tracks are 20 cm in width.

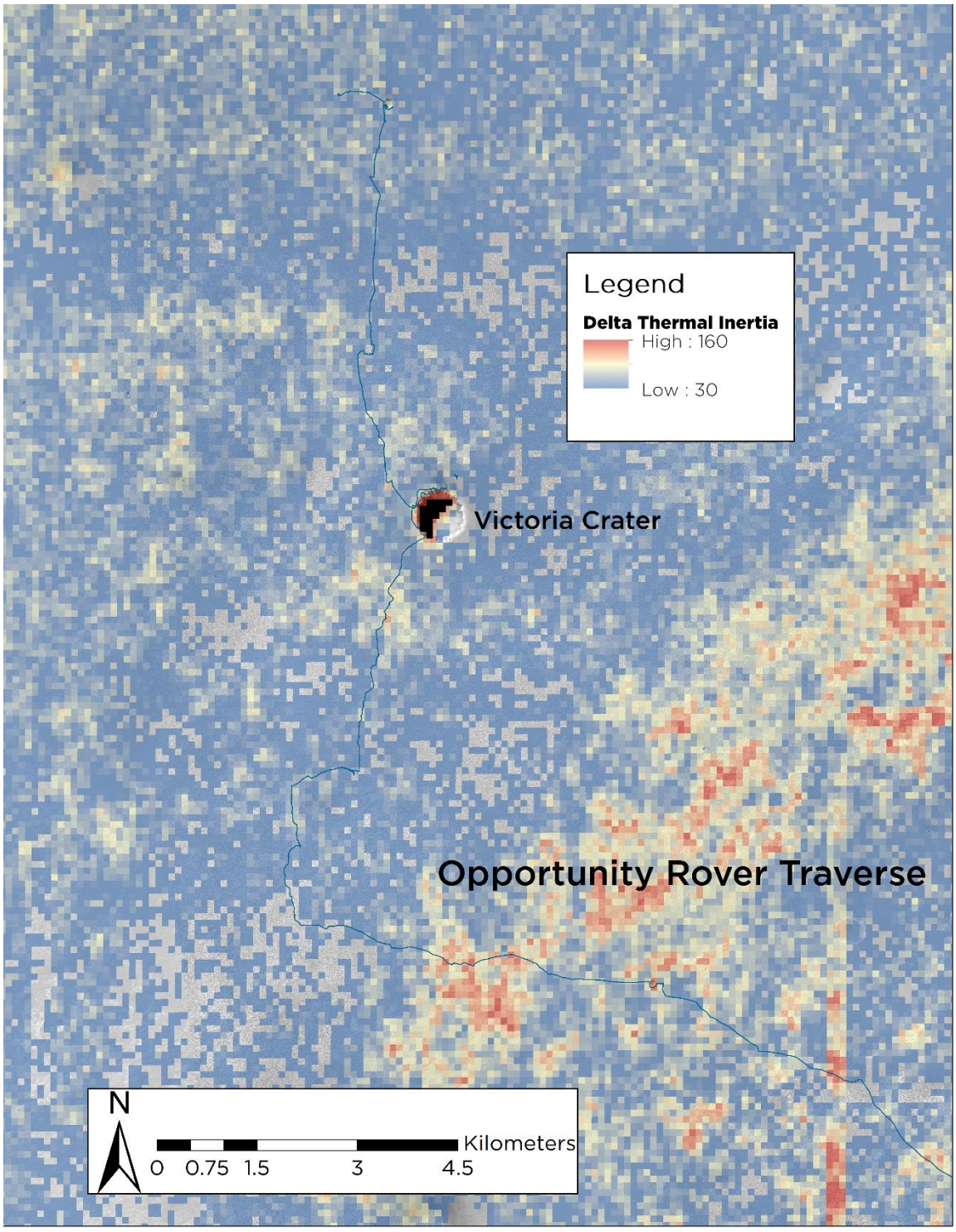

Figure 6. A view along the traverse of the Opportunity rover. Data scale ranges from a ΔI of 30 to 160. Note the excluded data around Victoria Crater which was avoided due to preferential thermal heating.

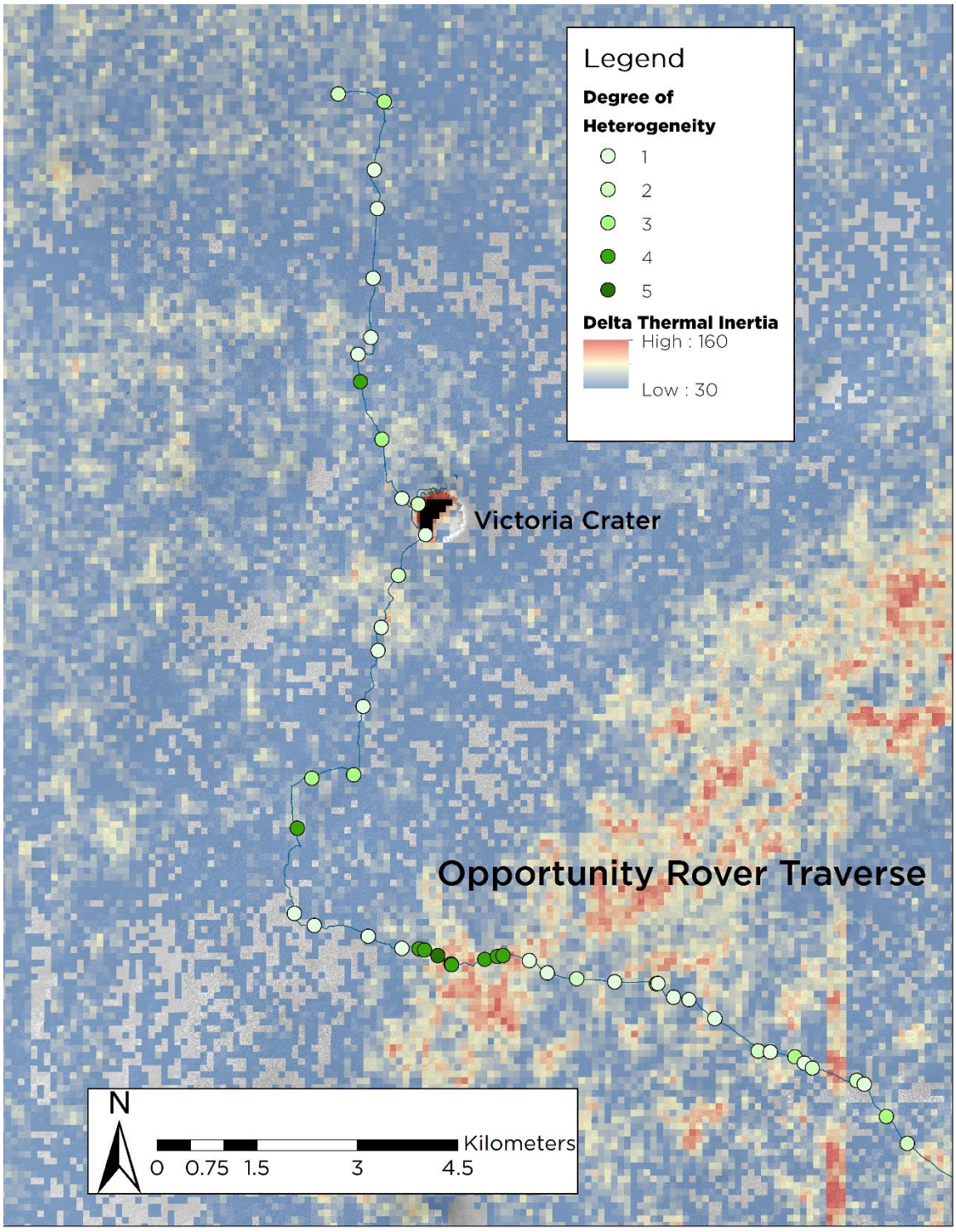

Figure 7. A view along the traverse of the Opportunity rover. Green points indicate locations which were evaluated by volunteers on the degree of heterogeneity. Larger circles indicate a higher ΔI.

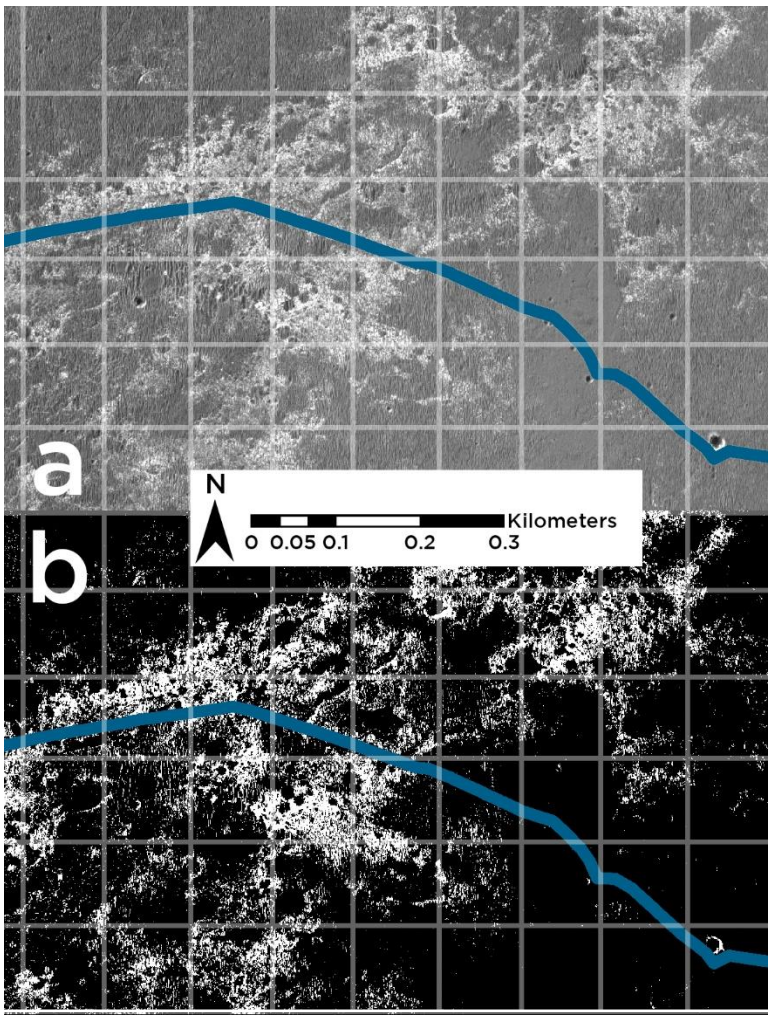

Figure 8. (a) Subset of a HiRISE image over a region of the Opportunity rover traverse. Note the lighter toned bedrock next to the darker toned sand. (b) Result of an image threshold of the above HiRISE image. The white represents outcrops of bedrock, where the black is dark sand. Grid pattern represents the resolution of a THEMIS pixel.

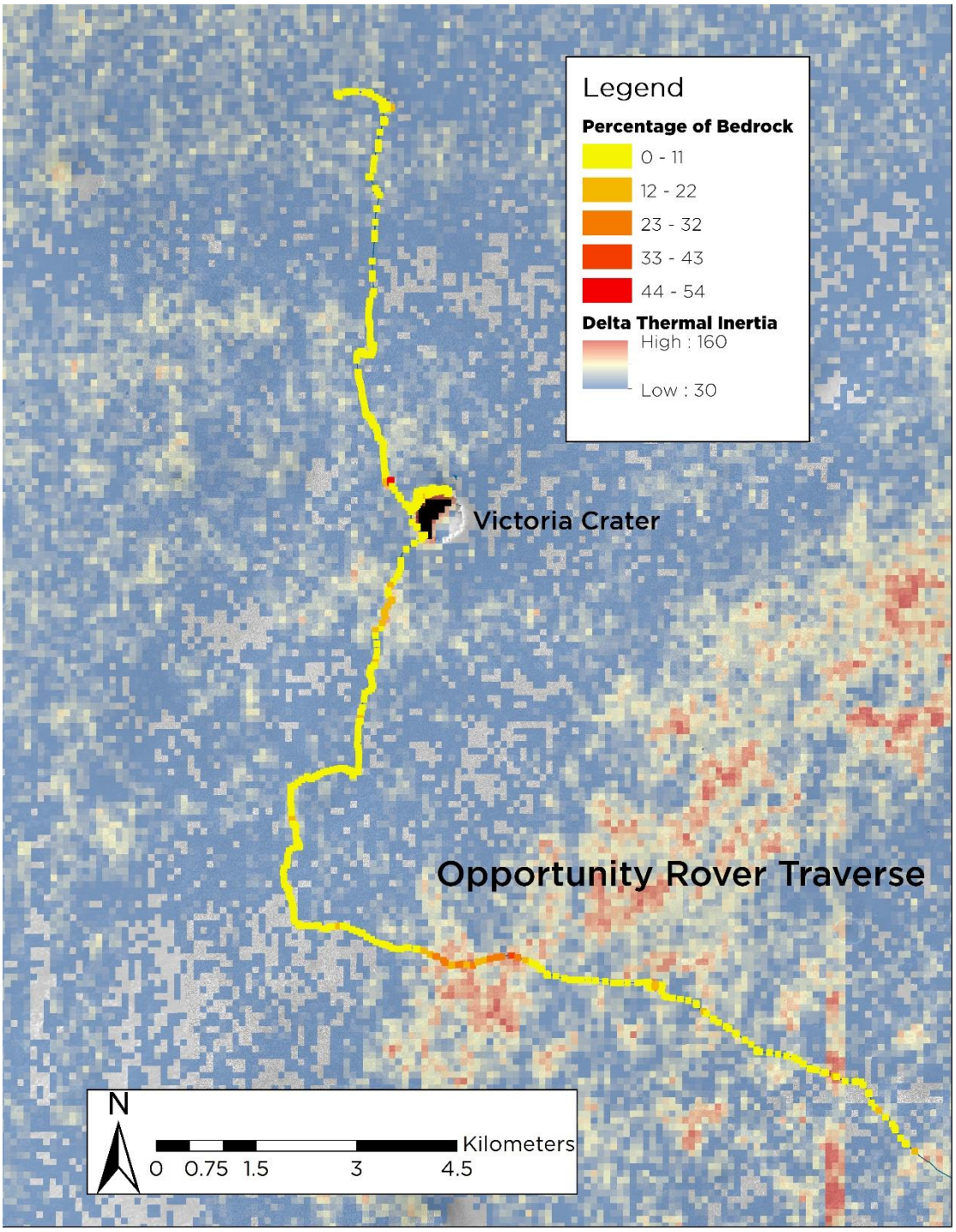

Figure 9. A view along the traverse of the Opportunity rover. Yellow to red points indicate the percentage of visible bedrock calculated over a 100-m buffer. Darker red indicate a larger percentage of bedrock.

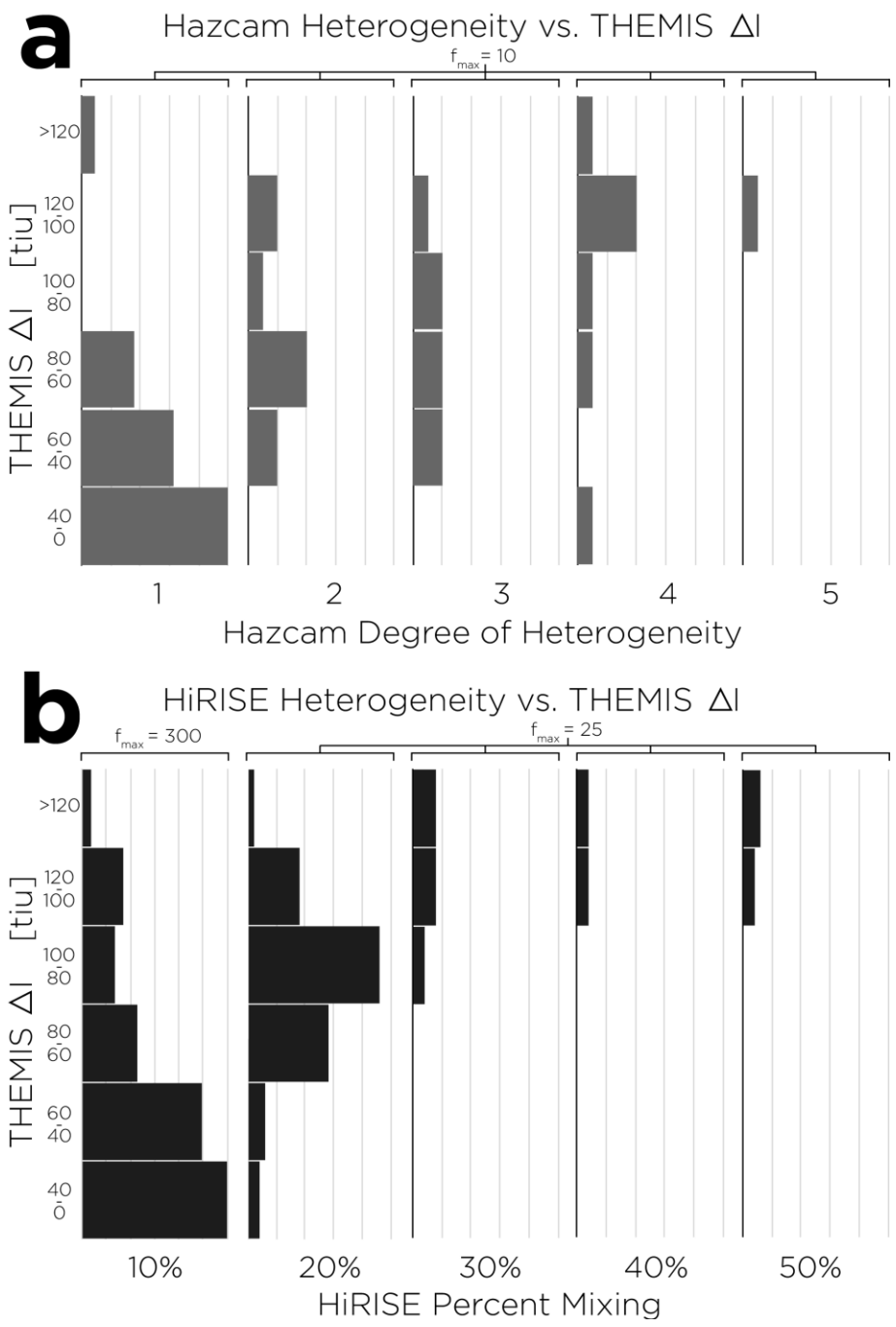

Figure 10. a) Comparison histogram of user submitted degree of heterogeneity via Hazcam images to the THEMIS calculated ΔI over the Opportunity *landing site in Meridiani Planum. b) Comparison histogram of percent mixing, as observed by HiRISE, compared to the change in apparent thermal observed by THEMIS over Meridiani Planum.* f_{max} *represents the maximum frequency value for each histogram.*

Appendix B: Theoretical Modeling of Diurnal Thermal Inertia Variations

Creation of a Lookup Table

Data used for lookup were collected through the KRC modeling program hosted by Arizona State University (Kieffer, 2013). These data are stored in a tab delimited text file. The first column is *albedo* which spans 0.01 to 0.2 and increments by 0.01. The second column is *thermal inertia*, which spans 12- to 2000-tiu in 1-tiu increments. The third and fourth columns are the results of the KRC program, which are the temperatures at *0400* (predawn) and *1400* (midday) LMST respectively.

21210	Albedo	TI	0400	1400
21211	0.11	1331.0	225.04	256.51
21212	0.11	1332.0	225.05	256.50
21213	0.11	1333.0	225.06	256.49
21214	0.11	1334.0	225.06	256.48
21215	0.11	1335.0	225.07	256.46
21216	0.11	1336.0	225.08	256.45
21217	0.11	1337.0	225.09	256.44
21218	0.11	1338.0	225.10	256.43
21219	0.11	1339.0	225.11	256.42
21220	0.11	1340.0	225.11	256.41
21221	0.11	1341.0	225.12	256.40
21222	0.11	1342.0	225.13	256.39
21223	0.11	1343.0	225.14	256.38
21224	0.11	1344.0	225.15	256.37
21225	0.11	1345.0	225.16	256.36

User Inputs

The program has no user inputs at the console, but at the end of the program file are several editable variables:

- Alb_sm Albedo of component 1
- Alb_lrg Albedo of component 2
- num Resolution of graph (default: 142)
- p_fine Percentage of component 1 to component 2

Program Outputs

Five matrices of *num* by *num* dimension consisting of the: predawn temperature (Celsius), midday temperature (Celsius), predawn thermal inertia (tiu), midday thermal inertia (tiu), and the ΔI values (tiu). All values within the matrix are equal to their corresponding x-value mixed in radiance space with the y-value in radiance space at the ratio defined by *p_fine*, afterwards combining back into temperature space.

Step 1: Search lookup table for temperature values

```
FUNCTION PRIMARY, P_sm, P_lrg, Alb_sm, Alb_lrg, p_fine, Albedo, Inertia, NightT, DayT, CoarseFine
    num=SIZE(Albedo, /N_ELEMENTS)-1

    ;////////////////////////////////////
    ;Matches Temperature to Initial Values
    ;\\\\\\\\\\\\\\\\\\\\\\\\\\\\\\\\\\\\
    FOR step2 = 0L, num DO BEGIN
        IF (Alb_sm EQ Albedo[step2]) AND (P_sm EQ Inertia[step2]) THEN BEGIN
            m_sm=step2
        ENDIF
        IF (Alb_lrg EQ Albedo[step2]) AND (P_lrg EQ Inertia[step2]) THEN BEGIN
            m_lrg=step2
        ENDIF
    ENDFOR
    Temp1 = NightT[m_sm] + 273
    Temp3 = DayT[m_sm] + 273
    Temp2 = NightT[m_lrg] + 273
    Temp4 = DayT[m_lrg] + 273
```

It should first be stated that a FOR loop is running the entire PRIMARY program. PRIMARY only calculates one ΔI for a specific point, therefore this loop calculates thermal inertia values individually at each step to generate the matrix. This section of the code above takes the two albedo values and two thermal inertia values and matches them to equal values in the lookup table. It then assigns four temperature variables to the predawn and midday temperatures for component 1 and B.

Step 2. Mixing temperatures in radiance space

Mixing temperatures must occur in radiance space, so the temperature variables are converted into radiance space using the PLANCKCAM subroutine. This is simply the Planck function manually added into IDL as the built-in function was slower.

$$B_\lambda(\lambda, T) = \frac{2hc^2}{\lambda^5} \frac{1}{e^{\frac{hc}{\lambda k_b T_1}} - 1}$$

The program runs the THEMISdata subroutine which takes the resultant temperature and combines it with the corresponding temperature for the other particle using the *p_fine* mixing ratio.

```
;////////////////////////////////
;Blackbody Curve with THEMIS bands
;\\\\\\\\\\\\\\\\\\\\\\\\\\\\\\\\
lambda   = [6.78, 7.93, 8.56, 9.35, 10.21, 11.04, 11.79, 12.57]
FWHM     = [1.01, 1.09, 1.16, 1.20, 01.10, 01.19, 01.07, 00.81]
avgNight = [1.0, 2.0, 3.0, 4.0, 5.0, 6.0, 7.0, 8.0]
avgDay   = [1.0, 2.0, 3.0, 4.0, 5.0, 6.0, 7.0, 8.0]
FOR i=0, 7 DO BEGIN
    avgNight[i] = THEMISDATA(Temp1, Temp2, lambda[i], p_fine, FWHM[i])
    avgDay[i]   = THEMISDATA(Temp3, Temp4, lambda[i], p_fine, FWHM[i])
ENDFOR


FUNCTION THEMISdata, Temp1, Temp2, Lam, p_fine, bandpass
    S_r1   = PLANCKCAM(Lam*1E-6, Temp1)
    S_r2   = PLANCKCAM(Lam*1E-6, Temp2)
    result = ((S_r1*(p_fine))+(S_r2*(1-p_fine)))
    RETURN, result
END


FUNCTION PLANCKCAM, Lam, T
    c     = 299792458.0
    e     = 2.718281828459
    h     = 6.626070040E-34
    kB    = 1.38064852E-23
    hhcc  = 1.1910429E-16
    hc    = 1.9864458E-25
    parta = (hhcc/(Lam^5))
    partb = 1/(e^((hc)/(Lam*kB*T))-1)
    rad   = parta*partb

    RETURN, rad
END
```

Step 3. Inverting the combined radiance

```
;////////////////////////////////////////
;Creating Function Closest to Planck Curve
;\\\\\\\\\\\\\\\\\\\\\\\\\\\\\\\\\\\\\\\\
DTempCalc = [1.0, 2.0, 3.0, 4.0, 5.0, 6.0, 7.0, 8.0]
NTempCalc = [1.0, 2.0, 3.0, 4.0, 5.0, 6.0, 7.0, 8.0]
FOR j=0, 7 DO BEGIN
    DTempCalc[j] = SOLVEFORT(lambda[j], avgDay[j])
    NTempCalc[j] = SOLVEFORT(lambda[j], avgNight[j])
ENDFOR
;print, DTempCalc
DayTemp   = MAX(DTempCalc) ;Delta T = 0.5
NightTemp = MAX(NTempCalc) ;Delta T = 1.0

IF (Alb_sm NE Alb_lrg) THEN BEGIN
    alb = (Alb_sm*p_fine)+(Alb_lrg*(1-p_fine))
    albdo = FLOAT(ROUND(alb*100)/100d)
ENDIF ELSE albdo = Alb_sm


FUNCTION SOLVEFORT, Lam, rad
    Temp = 1.9864458E-25/(((Lam*1E-6)*1.38064852E-23)*ALOG(1.1910429E-16/(rad*(Lam*1E-6)^5)+1))
    RETURN, Temp
END
```

This function takes the combined radiance and inverts the radiance equation to find the corresponding temperature.

```
;////////////////////////////////////
; Apply Forward Model to Lookup Table
;\\\\\\\\\\\\\\\\\\\\\\\\\\\\\\\\\\\\
minimumN = 1000.0
minimumD = 1000.0
FOR z=0L, num DO BEGIN
    numcheckN=ABS(NightT[z] - (NightTemp-273.0))
    numcheckD=ABS(DayT[z] - (DayTemp-273.0))
    IF (numcheckN LT minimumN) AND (albdo EQ Albedo[z]) THEN BEGIN
        rowMatchN = z
        minimumN = numcheckN
    ENDIF
    IF (numcheckD LT minimumD) AND (albdo EQ Albedo[z]) THEN BEGIN
        rowMatchD = z
        minimumD = numcheckD
    ENDIF
ENDFOR
```

Step 4. Link temperatures to the lookup table

Here the new temperatures are matched to every value within a similar albedo to find the closest match. This index value is saved and used later in the next step.

Step 5. Calculation of *ΔI*

The predawn thermal inertia (here listed as night) and midday thermal inertia are subtracted to generate the *ΔI* value. The midday temperature, predawn temperature, midday thermal inertia, predawn thermal inertia, and *ΔI* are all assigned to the *ThermInfo* variable.

```
    ;////////////////////////////////
    ; Temperature Interpolation Routine
    ;\\\\\\\\\\\\\\\\\\\\\\\\\\\\\\\\
    NT1 = NightT[rowMatchN-1]
    NT2 = NightT[rowMatchN]
    NPR = ((NightTemp-273)-NT1)/(NT2-NT1)
    DT1 = DayT[rowMatchD-1]
    DT2 = DayT[rowMatchD]
    DPR = ((DayTemp-273)-DT1)/(DT2-DT1)

    NI = NPR*(Inertia[rowMatchN]-Inertia[rowMatchN-1])+Inertia[rowMatchN-1]
    DI = DPR*(Inertia[rowMatchD]-Inertia[rowMatchD-1])+Inertia[rowMatchD-1]
    P_delta = (DI-NI)
    ThermInfo = {info, DayTemp:DayTemp-273, NightTemp:NightTemp-273, DayInert:DI, NightInert:NI, DeltaInert:P_delta}
    ;ThermInfo = P_delta

    RETURN, ThermInfo
END
```

Step 6. Assign each temperature value into a matrix

```
Pro LARGEMATRIX4
sTimeS = SYSTIME(/seconds)
;////////////////////////////////////////
;Places Lookup Table into Various Arrays
;\\\\\\\\\\\\\\\\\\\\\\\\\\\\\\\\\\\\\\\\
READCOL, 'D:\Cameron\Google Drive\Research\LookupTable2.txt', F=' ', Albedo, Inertia, NightT, DayT


;////////////////////////////////
;////////////////////////////////
;       CHANGE THESE VALUES
;\\\\\\\\\\\\\\\\\\\\\\\\\\\\\\\\
;\\\\\\\\\\\\\\\\\\\\\\\\\\\\\\\\

Alb_sm = 0.10
Alb_lrg = 0.10
num=142


;////////////////////////////////////////
;////////////////////////////////////////
;             CODE TO RUN
;\\\\\\\\\\\\\\\\\\\\\\\\\\\\\\\\\\\\\\\\
;\\\\\\\\\\\\\\\\\\\\\\\\\\\\\\\\\\\\\\\\

xresolution=float(num)
CoarseFine = 2
A = MAKE_ARRAY(num+2, num+2, /STRING)
B = MAKE_ARRAY(num+2, num+2, /STRING)
C = MAKE_ARRAY(num+2, num+2, /STRING)
D = MAKE_ARRAY(num+2, num+2, /STRING)
E = MAKE_ARRAY(num+2, num+2, /STRING)


FOR Y=0, xresolution DO BEGIN
    P_sm = 12+(14*(Y))
    FOR X=0, xresolution DO BEGIN
        P_lrg = 12+(14*(X))
        p_fine=0.0
        IF (Y LT X) THEN BEGIN
            ThermInfo = {double, DayTemp:0, NightTemp:0, DayInert:0, NightInert:0, DeltaInert:0}
            ;ThermInfo = 0
        ENDIF ELSE BEGIN
            ThermInfo = PRIMARY(P_sm, P_lrg, Alb_sm, Alb_lrg, p_fine, Albedo, Inertia, NightT, DayT, CoarseFine)
        ENDELSE
        A[X,Y]=STRING(ThermInfo.NightTemp)+','
        B[X,Y]=STRING(ThermInfo.DayTemp)+','
        C[X,Y]=STRING(ThermInfo.DayInert)+','
        D[X,Y]=STRING(ThermInfo.NightInert)+','
        E[X,Y]=STRING(ThermInfo.DeltaInert)+','
    ENDFOR
ENDFOR
```

Vita

Cameron Blake McCarty was born in Seoul, South Korea on March 12, 1992 to David and Crisa McCarty. Cameron lived there briefly before moving to Michigan. There Cameron attended Ottawa Montessori Academy, a unique school which was the first to develop a lifelong joy of learning and quest for knowledge in him. His teacher, Dottie Gretzinger, encouraged interest in science and math long before the days of STEM. After 3rd grade, Cameron and his family moved to Columbus, Georgia. Cameron's father, a 3D animator was employed at the Coca-Cola Space Science Center (a job offer for which Cameron and his mother strongly advocated). The Science Center soon became his home, after school he would roam the main lobby, and read every exhibit. In 2003 the opposition of Mars occurred, and hundreds of guests came to the Science Center to observe. Short-staffed, the director, Shawn Cruzen, placed 11-year-old Cameron on a telescope to help. The Science Center was Cameron's first volunteer job, paid job, internship, and yes, first place from which to be terminated (he was later re-hired). Cameron graduated from Hardaway High School in 2010 and attended Columbus State University as an Earth and Space Science major (as one of the first graduates of the degree). He was offered and accepted two internships at the Marshall Space Flight Center, in Huntsville, Alabama. The first was investigating the dust flux from comets and predicting damage estimates for the soon-to-arrive MAVEN mission. The second was creating a new algorithm for the identification of grains in lunar thin sections. Image analysis began to really interest him, so when offered the opportunity to attend the University of Tennessee and work on remote sensing with Dr. Jeff Moersch, Cameron happily accepted. At UT, Cameron has been a Payload Uplink Lead for the Mars Exploration Rover, trekked across Iceland mapping volcanoes, and hiked around Meteor Crater to map ejecta.